Characterization of $Mn_{0.67}Zn_{0.33}Fe_2O_4$ nanoparticles synthesized under different pH

Rodrigo Uchida Ichikawa[1,a], Walter Kenji Yoshito[1,b], Margarida Juri Saeki[2,c], Willian C. A. Maranhão[1,d], Fátima Goulart[1,e] and Luis Gallego Martinez[1,f]

[1]*Instituto de Pesquisas Energéticas e Nucleares, Av. Prof. Lineu Prestes, 2242 - Cidade Universitária, São Paulo - SP, 05508-000, Brazil.*

[2]*Instituto de Biociências, Universidade Estadual Paulista "Júlio de Mesquita Filho", Distrito de Rubião Junior, s/n, Botucatu - SP, 18618-970, Brazil.*

[a]*ichikawa@usp.br*, [b]*wyoshito@ipen.br*, [c]*mjsaeki@ibb.unesp.br*, [d]*maranhao@usp.br*, [e]*amitafis@hotmail.com*, [f]*lgallego@ipen.br*

Keywords: Mn-Zn ferrite nanoparticles, X-ray diffraction, X-ray fluorescence, thermal analysis, dynamic light scattering, scanning electron microscopy.

Abstract. Nanostructured Mn-Zn ferrites were synthesized using co-precipitation in alkaline solution with different pH. The samples were characterized using X-ray diffraction (XRD), X-ray fluorescence (XRF), thermal analysis (TG-DTA), dynamic light scattering (DLS) and scanning electron microscopy (SEM) techniques. Monophasic nanoparticles were formed when synthesized with pH 10.5. This sample was heat-treated and its XRD data was refined by the Rietveld method. Mean crystallite sizes and microstrains were determined from X-ray line profile analysis using Single-Line and Warren-Averbach methods, which revealed a mean crystallite size of approximately 10 nm and negligible microstrains. Zn content was estimated using refined cell parameters, giving a value of 33 at %, in accordance with XRF result. TG-DTA revealed that the incorporation of α-Fe_2O_3 occurs around 1130 °C and 1200 °C with recrystallization of the Mn-Zn ferrite spinel phase. DLS showed that mean particle size increase with temperature up to 1159 nm at 800 °C. SEM analysis showed the samples agglomerate and present similar morphology with negligible size changing when calcined between 280 °C and 800 °C. However, the sample calcined at 1200 °C presents larger agglomerates due to the sintering process.

Introduction

Manganese-zinc ferrites are key technological materials due to their unique properties, such as high initial magnetic permeability, high resistivity and low hysteresis loss [1,2]. More recently, nanostructured Mn-Zn ferrites have been applied in medical procedures, such as magnetic carriers for bioseparation, enzymes and proteins immobilization and as marker in the diagnosis of several diseases [1]. Magnetic and electrical properties of these nanoparticles are closely related to their crystal structure and microstructure, therefore, the characterization of their properties and behavior under temperature changes is of utmost importance [2,3].

In this study Mn-Zn ferrite nanoparticles were synthesized by the co-precipitation, using different pH for the precipitating solution and characterized by X-ray powder diffraction (XRD), X-ray fluorescence (XRF), thermal analysis (TA), dynamic light scattering (DLS) and scanning electron microscopy (SEM) techniques. The crystal structure was modeled using Rietveld analysis and the microstructure characterization was performed by Single-Line [4] and Warren-Averbach [5] methods to determine mean crystallite size, microstrain and crystallite size distribution.

Experimental

$Mn_{0.67}Zn_{0.33}Fe_2O_4$ nanoparticles were synthesized by wet chemical co-precipitation, using analytical grade manganese chloride tetrahydrate ($MnCl_2.4H_2O$), zinc chloride ($ZnCl_2$) and iron chloride hexahydrate ($FeCl_3.6H_2O$). The salts were dissolved in de-ionized water to obtain free Fe^{3+}, Mn^{2+} and Zn^{2+} ions solution. This solution was dropped into alkaline solutions, containing

sodium hydroxide (NaOH) to obtain the desired pH (9.5, 10.5 and 12.0). The co-precipitations were performed under vigorous stirring and heating at 95 °C. Resulting powders were vacuum-filtered and washed with distilled water to remove sodium and chloride ions and dried at 70 °C for 24 h.

The samples were characterized by thermal analysis (Thermobalance Setaram Labsys Instrumentation, TG-DTA/DSC) under dynamic air and heating rate of 10 °C.min^{-1} in alumina crucibles. The particle size distribution was obtained by dynamic light scattering (ZetaPALS-Zeta Potential Analyzer) in aqueous suspensions with 0.1% w/w of solid.

X-ray diffraction data was collected with Bragg-Brentano geometry (Rigaku Ultima IV) with CuKα radiation. The measurements were performed in the 2θ range of 10° up to 100°, at 0.02° steps and 20 sec/step counting time. The divergence, antiscatter and receiving slits were set to 1/2°, 1/2° and 0.3 mm, respectively. X-ray fluorescence measurement was performed with a Shimadzu EDX-720 spectrometer using 50 kV and 100 mA with a 1.0 mm beam.

Structural parameters were determined by Rietveld refinement using the software *TOPAS 4.2* [5]. Mean crystallite sizes and microstrains were determined using Single-Line (SL) [3] and Warren-Averbach (WA) methods [4] using a procedure described in a previous work [7]. The crystallite sizes distribution can be determined using the results of both methods [6,7]. For this determination, it was assumed that the crystallite size distribution follows a lognormal distribution and the crystallites have spherical shape.

Results and discussion

In Fig. 1a XRD patterns for the samples synthesized with different pH are presented. It can be observed that all samples present mainly the desired spinel ferrite phase (peaks indicated with F). However, secondary phases were found for the samples synthesized at pH 9.5 and 12.0, being one of them α-Fe_2O_3 (peaks indicated as H) and the other a non-identified phase (indicated with *). These non-identified phase peaks can be related to either Fe or FeO, however some peaks of these phases can be overlapped with those of the main phase and the identification is hampered.

The particle sizes of samples synthesized with pH 9.5, 10.5 and 12.0, were analyzed in neutral pH by DLS and the distribution can be seen in Fig. 1b. Considering the crystallite sizes determined from X-ray diffraction data (Table 2), it can be verified that the particles are in fact formed by agglomeration of grains. In the cumulative size distribution ($D_{10,}$ D_{50} and D_{90}), presented in Table 1, it can be seen that the agglomerate sizes increase with pH. This is an indication that the pH of the precipitating solution can influence the surface properties of the material.

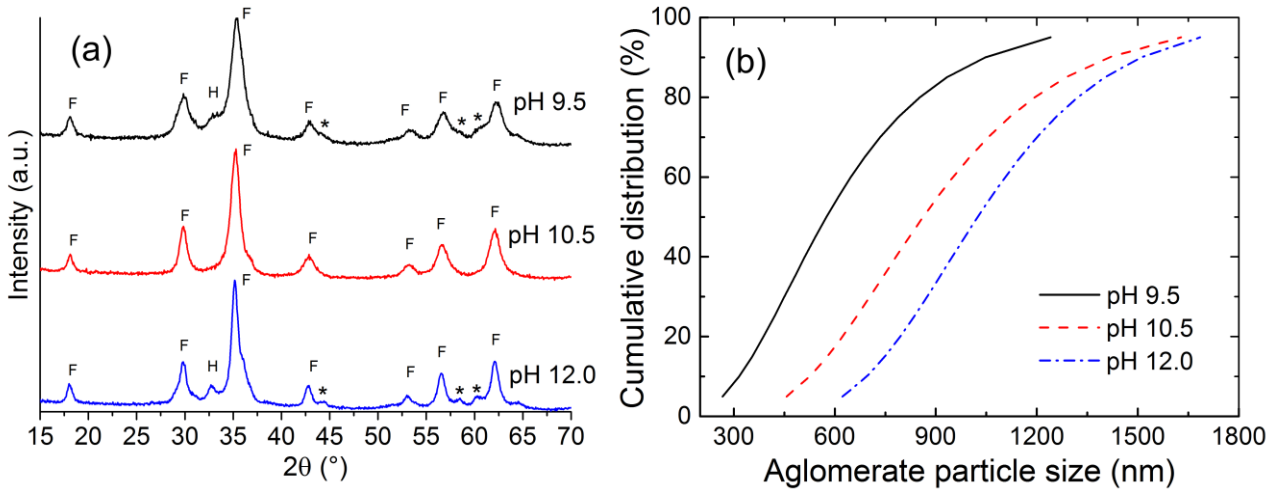

*Figure 1. (a) XRD profiles of Mn-Zn ferrites prepared by co-precipitation with different pH. Peaks labeled F indicate those related to $Mn_{0.75}Zn_{0.25}Fe_2O_4$ spinel phase (ICSD 28515), H to α-Fe_2O_3 (ICSD 66756) and * for non-identified phases and (b) Particle size distribution.*

Table 1. Cumulative agglomerate size distribution of Mn-Zn ferrite synthesized with pH 9.5, 10.5 and 12.0.

pH	9.5	10.5	12.0
D_{10} [nm]	320	527	697
D_{50} [nm]	575	863	1024
D_{90} [nm]	1052	1430	1522

The subsequent analysis was performed only for the sample synthesized at pH 10.5, since peaks of secondary phases can give biased results.

The lattice parameter value obtained by Rietveld refinement for the sample synthesized at pH 10.5 (Fig. 2a) was 0.8442(3) nm with a R_{wp} of 5.1%. Using a plot of lattice parameter versus the Zn concentration from a study performed by Rath et al. [8], adapted in Fig. 2b, we can estimate the Zn content of this sample as being about ~~0.~~33 at %, in accordance with the nominal value. This result is higher than the value determined by XRF of ~~0.~~28 at %. This difference can be attributed to the difference in the synthesis methods. In the study by Rath et al. [8] it was used hydrothermal synthesis at 180 °C to prepare the ferrites, which can provide distinct cation distribution in the spinel, relatively to co-precipitation method [9,10] used in our study. The difference may also be due to the composition so that the more crystalline portion of the particles is richer in Zn (33 at %) and the other portion is amorphous with lower content of Zn, giving an average of 28%. The difference in composition may result from the dissolution of Zn in the form of coordination compounds.

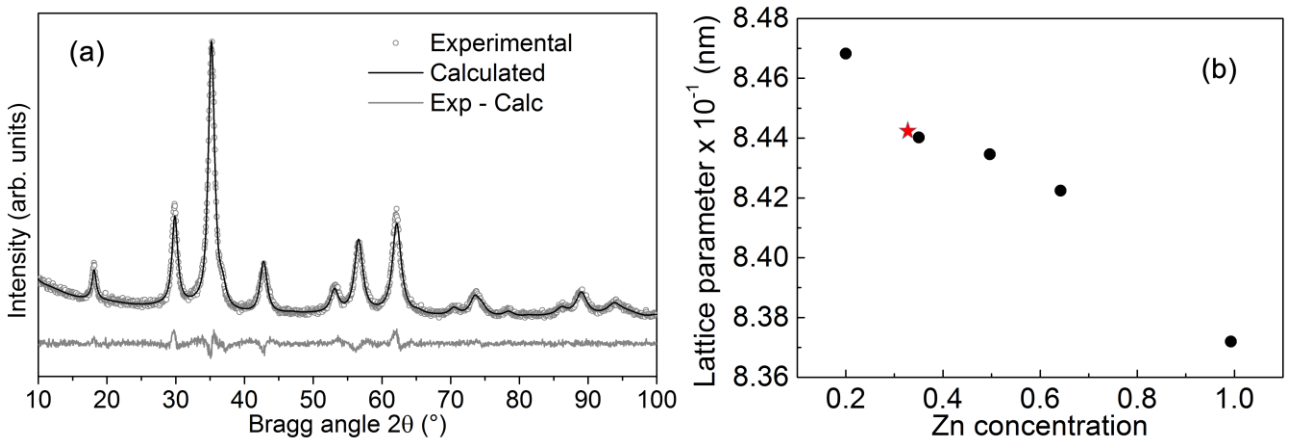

Figure 2. (a) Rietveld refinement for the Mn-Zn ferrite sample synthesized with pH 10.5. (b) Lattice parameter versus Zn concentration. In black circles: values from the study done by Rath et al. [8]; red star: value obtained for the Mn-Zn ferrite in our study.

Mean crystallite sizes were determined using Single-Line (SL) [4] and Warren-Averbach (WA) [5] methods using (022) and (044) planes reflections according to a procedure described in a previous work [7]. The mean crystallite size given by SL is a volume-weighted mean value (L_V), while the Warren-Averbach method provides an area-weighted mean value (L_A). It was obtained for L_A and L_V, 8.7(5) and 11.1(3) nm, respectively and a root mean square strain (RMSS) of 5.1×10^{-3}. The RMSS value is low, which indicates that the sample presents negligible microstrain. Using both, L_A and L_V it is possible to determine the crystallite size distribution [8]. For this study, it was assumed crystallites with spherical shape and a lognormal distribution. The crystallite size distribution revealed narrow dispersion of sizes, with mean value of 10.1 nm and standard deviation of 3.7 nm.

Thermal analysis was performed on the sample in order to determine the temperatures where transformations occur (Fig. 3a). The thermogravimetric evolution from ambient temperature to 1200 °C shows a continuous decreasing corresponding to water loss. The simultaneously obtained DTA curve shows an endothermic process up to 100 °C, which can be attributed to water evaporation. The exothermic process from 100 °C to 200 °C is due to the decomposition of

hydroxides, described by the Eq's. 1 and 2 for the lower range of temperature and Eq. 3 near to 200 °C and spinel phase crystallization. (se tiver referências para citar aqui, seria bom)

$$M(OH)_2 \rightarrow MO_{spinel} + H_2O \ (M = Mn \text{ and } Zn) \quad (1)$$

$$2Fe(OH)_3 \rightarrow 2FeO(OH) + 2H_2O \quad (2)$$

$$2FeO(OH) \rightarrow Fe_2O_{3\ spinel} + H_2O \quad (3)$$

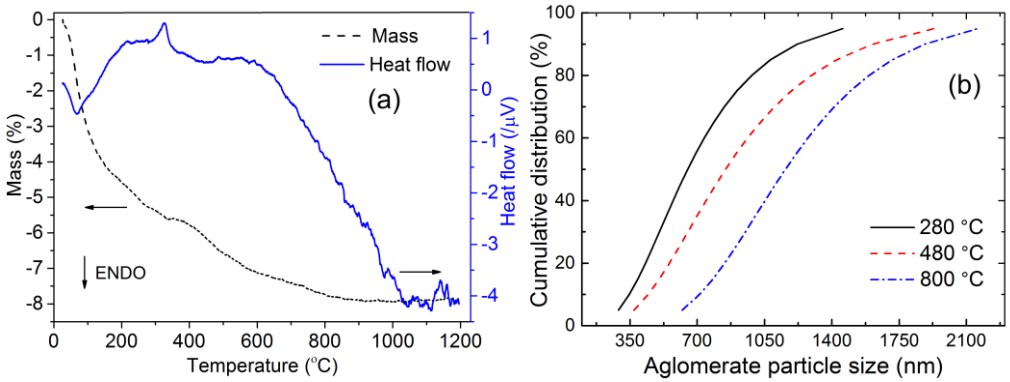

Figure 3. (a) Thermal analysis, TG and DTA of Mn-Zn-ferrite and (b) particle size distribution of Mn-Zn ferrite synthesized with pH 10.5 after heat-treatments.

In the DTA curve, the peak at approximately 325 °C corresponds to the segregation of hematite phase (α-Fe_2O_3), which corroborates with the plateau on the TGA curve. Between 1130 °C and 1200 °C occurs the incorporation of α-Fe_2O_3 and recrystallization of the Mn-Zn ferrite spinel phase [1] as evidenced by XRD (Fig. 5). Based on these analyses, the sample was heat-treated at 280 °C, 480 °C and 800 °C in air and analyzed by dynamic light scattering (DLS) to determine particle sizes distributions. Results for cumulative distributions are presented in Fig. 3b. Mean particle sizes (MS) and polydispersity index (PI) are summarized in Table 2.

Table 2 - Mean particle *sizes (MS) and polydispersity index (PI) of Mn-Zn ferrite synthesized with pH 10.5 and heat-treated at 280 °C, 480 °C and 800 °C.*

Sample	MS (nm)	PI
280 °C	654	0.280
480 °C	852	0.277
800 °C	1159	0.184

From the results presented in Table 2 the MS increase with temperature, which indicates that the particles agglomerate with increasing temperature. On the other hand, the PI decreases with temperature, indicating that the distribution becomes narrower with increasing temperature. The values between 0.184 and 0.280 indicate a moderate size distribution. The heat-treated samples were then analyzed by SEM. The images presented in Fig. 4 show that agglomerates with similar morphology form when the samples are calcined between 280 °C and 800 °C, i.e., it forms soft agglomerates and its sizes does not increase with temperature. However, the sample calcined at 1200 °C contains dense particles with larger sizes, due to the sintering.

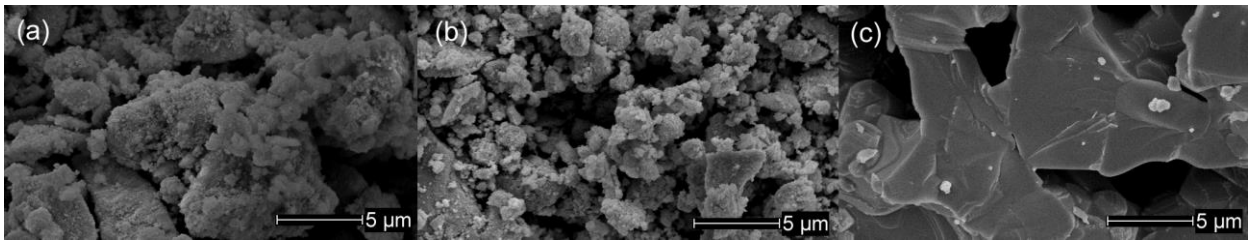

Figure 4. SEM images of Mn-Zn ferrite powders heat-treated at: (a) 280 °C, (b) 800 °C and (c) 1200 °C.

XRD patterns for the as-synthesized and heat-treated Mn-Zn ferrite samples are presented in Fig. 5a. It can be observed that the heat treatment at 280 °C promotes segregation of α-Fe_2O_3 phase and that treatments at 480 °C and 800 °C were not effective to eliminate this secondary phase, although a crystallite growth, evidenced by the narrowing of peaks, can be observed. However, α-Fe_2O_3 was not observed when the sample was treated at 1200 °C. This can be attributed to the incorporation of α-Fe_2O_3 by the spinel phase exhibiting a well crystallized cubic spinel-ferrite at this temperature [1,10]. Some samples presented also a small contamination of SiO_2, probably from the borosilicate experimental apparatus used in the synthesis. Rietveld analysis has provided the results for cell parameters, phase density, mean crystallite size and microstrain for all samples. Results are presented in Table 3 and a plot of mean crystallite size and microtrain; cell parameters and density versus temperature in Fig. 5b. Mean crystallite size (D) and microstrain (e_0) definitions can be seen in the work of Balzar et al. 2004 [11].

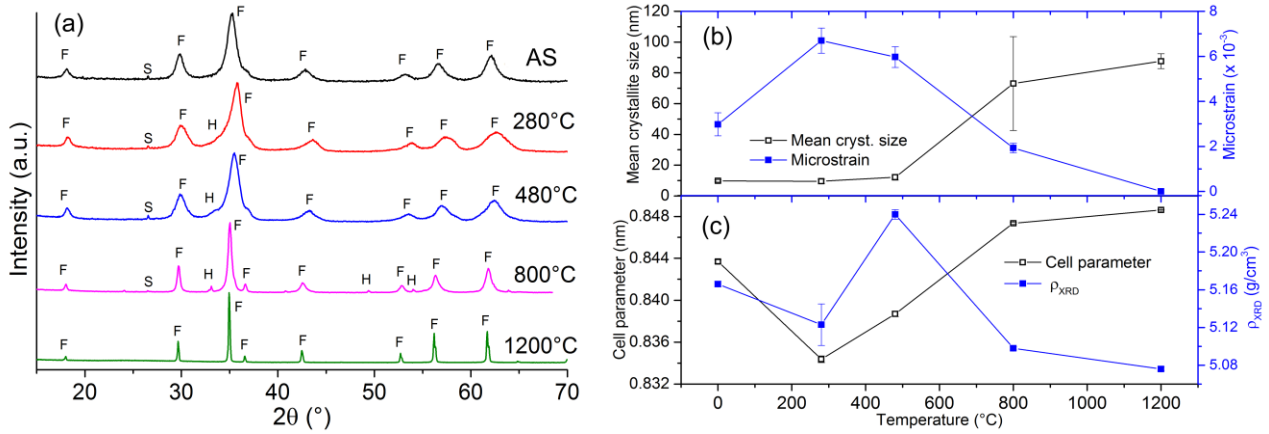

Figure 5. (a) XRD profiles for the as-synthesized and heat-treated Mn-Zn ferrite samples obtained using pH 10.5. F stands for M-Zn ferrite, S for SiO_2 and H for α-Fe_2O_3. (b) mean crystallite size/microstrain and (c) cell parameter/density of Mn-Zn ferrite samples versus temperature.

Table 3 – Cell parameters (a), density (ρ_{XRD}), mean crystallite size (D) and microstrain (e_0) by Rietveld refinement of XRD data.

Sample	a (nm)	ρ (g/cm^3)	D (nm)	e_0	Rwp (%)
AS	0.84369 (17)	5.166 (3)	9.8 (0.8)	0.00298 (51)	5.9
280°C	0.83437 (32)	5.123 (22)	9.5 (1.3)	0.00670 (56)	11.6
480°C	0.83869 (26)	5.240 (5)	12.1 (1.8)	0.00597 (46)	11.2
800°C	0.84736 (10)	5.098 (2)	73.1 (30.5)	0.00193 (21)	11.8
1200°C	0.84862 (1)	5.076 (2)	87.6 (4.8)	0	14.0

The treatment at 280 °C induced an increase in the microstrain, which was eliminated after treatment at higher temperatures, followed by an increase of mean crystallite sizes as expected. Also, a slight cell parameter and density decrease can be seen at 280 °C followed by an increase of cell parameter for higher temperatures. Density reaches its maximum at 480 °C to decrease after. This is due to segregation of α-Fe_2O_3 phase and to the elimination of hydroxides and crystallization, as confirmed by the exothermic peak at 280 °C in the DTA curve. From 480 °C to 1200 °C is observed a continuous increase of cell parameter and decrease of density.

Conclusions

It was possible to conclude that the pH of 10.5 is the better condition to prepare monophasic Mn-Zn ferrite nanoparticles. Using the lattice parameter obtained by Rietveld refinement, the Mn-Zn ferrite composition was estimated as $Mn_{0.67}Zn_{0.33}Fe_2O_4$. Nanosized particles were successfully

obtained as confirmed by size-strain analysis using Single-Line and Warren-Averbach methods. Crystallite size distribution presented a narrow distribution around 10 nm. TG-DTA showed an endothermic process up to 100 °C (water evaporation) and an exothermic process from 100 °C to 200 °C (decomposition of hydroxides and spinel phase crystallization). Segregation of α-Fe_2O_3 occurs at approximately 325 °C but it was incorporated at 1130 °C and 1200 °C, where recrystallization of the Mn-Zn ferrite spinel phase occurred. DLS showed that the polydispersity of the sample decreases with temperature and that the particle tends to agglomerate with increasing temperature. SEM revealed soft agglomerates when calcined between 280 °C and 800 °C, however, its size does not increase with temperature. Nevertheless, when calcined at 1200 °C, dense particles with larger sizes are observed. Lastly, the heat-treatment at 280 °C increased the microstrain, which was eliminated at higher temperatures, followed by an increase of mean crystallite size up to 87.6 (4.8) nm.

Acknowledgments

The authors acknowledge CAPES for R.U. Ichikawa scholarship, CNPq (# 206983/2014-0) for financial support, Dr. V. L. R. Salvador for XRF analysis and IPEN's Electron Microscopy Lab, Rheology Lab. and Fuel Cell and Hydrogen Center.

References

[1] P. Hu, H. Yang, D. Pan, H. Wang, J. Tian, S. Zhang, X. Wang, A. A. Volinsky, Heat treatment effects on microstructure and magnetic properties of Mn–Zn ferrite powders. J. Magn. Magn. Mater. 322 (2010) 173-177.

[2] M. Syue, F. Wei, C. Chou, C. Fu, Magnetic, dielectric, and complex impedance properties of nanocrystalline Mn–Zn ferrites prepared by novel combustion method, Thin Solid Films. 519 (2011) 8303–8306.

[3] Th. H. de Keijser, J. I. Langford, E. J. Mittemeijer, A. B. P. Vogels, Use of the Voigt function in a single-line method for the analysis of X-ray diffraction line broadening. J. Appl. Cryst. 15, (1982) 308-314.

[4] B. E. Warren, B. L. Averbach, The Effect of Cold Work Distortion on X-Ray Patterns. J. Appl. Phys. 21 (1950) 595-599.

[5] A. Coelho. Topas Academic Version 4.1. Computer Software, Topas Academic, Coelho Software, Brisbane, 2007.

[6] R. U. Ichikawa, L. G. Martinez, K. Imakuma, X. Turrillas, Development of a methodology for the application of the Warren-Averbach method, in: Anais do V Encontro Científico de Física Aplicada, n.1, v.1. São Paulo: Blucher, 2014, p. p107-110.

[7] C. E. Krill, R. Birringer, Estimating grain-size distributions in nanocrystalline materials from X-ray diffraction profile analysis, Philos. Mag. A. 77 (1998) 621-640.

[8] C. Rath, S. Anand, R. P. Das, K. K. Sahu, S. D. Kulkarni, S. K. Date, N. C. Mishra, Dependence on cation distribution of particle size, lattice parameter, and magnetic properties in nanosize Mn-Zn ferrite, J. Appl. Phys. 91 (2002) 2211-2215.

[9] R. D. Shannon, C.T. Prewitt, Effective ionic radii in oxides and fluorides, Acta Cryst. B, 25 (1969) 925-946.

[10] H. St. C. O'Neill, A. Novrotsky, Simple spinels: crystallographic parameters, cation radii, lattice energies, and cation distribution, Am. Mineral. 68 (1983) 181-194.

[11] D. Balzar, N. Audebrand,M. R. Daymond, A. Fitch, A. Hewat, J. I. Langford, A. Le Bail, D. Louër, O. Masson, C. N. McCowan, N. C. Popa, P.W. Stephens, B. H. Toby. Size–strain line-broadening analysis of the ceria round-robin sample, J. Appl. Cryst. 37 (2004) 911–924.